Results in Engineering 30 (2026) 109755

Contents lists available at ScienceDirect

Results in Engineering

journal homepage: www.sciencedirect.com/journal/results-in-engineering

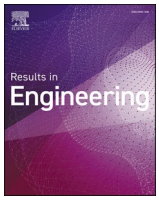

Research paper

Establishment of standardized intraoral implant model in the rabbit edentulous diastema

Xinning Dai [a,†], Xiaoqiong Huang [a,†], Xinwen Deng [a,†], Zhiqian Ye [a], Zixiang Liu [a], Weiran Li [a], Yan Li [a], Shuyi Wu [a,*], Shujin Li [a,b,*]

[a] Hospital of Stomatology, Guanghua School of Stomatology Guangdong Provincial Key Laboratory of Stomatology, Sun Yat-sen University, Guangzhou 510055, PR China

[b] Division in Anatomy and Developmental Biology Department of Oral Biology, Taste Research Center, Oral Science Research Center BK21 FOUR Project, Yonsei University College of Dentistry, Seoul, 03722, South Korea

ARTICLE INFO

Keywords:
Intraoral implant model
Rabbit edentulous diastema
Standardization
Peri-implantitis

ABSTRACT

Rabbits have been valued for decades as a model for osseointegration research and biomaterial evaluation, owing to the practical handling, ethical acceptance, and cost-effectiveness. The rabbit model provides an optimal compromise between clinical translatability and practical experimental viability when compared to both large-animal and rodent alternatives. However, rabbit models face inconsistencies across implant site selection criteria, implant geometric configurations, and operative techniques, underscoring the urgent need for standardized experimental frameworks to improve cross-study comparability. The edentulous diastema in rabbit mandible—an anatomical edentulous zone between incisors and premolars—is recognized as a promising intraoral site for implant placement due to its enhanced trabecular bone density and superior volumetric capacity. In contrast to commonly used extragnathic sites (e.g., tibia, femur), which lack a relevant oral microenvironment, the mandibular diastema offers both close anatomical analogy to the human jaw and straightforward surgical access. Herein, we identified an anatomically optimal implant site in rabbit mandibular edentulous diastema utilizing micro-CT-based quantitative analyses and designed a customized implant according to the measured value. Subsequently, we developed a standardized operative workflow for implant placement, and evaluated the osseointegration following 4 weeks and 12 weeks of implantation. Furthermore, we confirmed the applicability of the standardized rabbit intraoral implant model for peri-implantitis modeling. Collectively, we established a workflow for standardizing an intraoral implant model in the edentulous diastema of rabbits which provide highly reproducible, economical, and effective platform for fundamental inquiries into osseointegration, the evaluation of novel implant surface coatings, and the initial screening of biomaterials.

1. Introduction

Animal models serve as critical tools in addressing three fundamental issues of implant dentistry: toxicological evaluation of biomaterials, biocompatibility assessment at the implant-tissue interface, and iterative optimization of implant materials and designs [1,2].

Currently, the most commonly used animals for establishing implant models include rats, dogs, sheep, pigs and rabbits, each of which presents distinct advantages and limitations [3]. Although rodents are widely used in implant research because of their low cost, rich genetic-modification tools, and rapid bone turnover, their diminutive skeleton lacks a Haversian system, undergoes lifelong mandibular growth, and cannot accommodate standard-diameter dental implants, creating a biomechanical environment markedly different from the human jaws. Rodents also present distinct metabolic and enzymatic profiles. Therefore, rodents are considered unsuitable for evaluating the biological and biomechanical endpoints of osseointegration [4,5]. The canine jaws could provide abundant bone volume and their bone density are similar to human. Their well-established histological standards could also provide robust long-term data. Nevertheless, ethical restrictions are stringent, approval cycles are lengthy, and husbandry plus anesthesia costs are high. Lifelong eruption of anterior teeth can produce

* Corresponding authors.
E-mail addresses: lishj88@mail.sysu.edu.cn (S. Wu), wushuyi@mail.sysu.edu.cn (S. Li).
† These authors contributed equally to this work and share first authorship.

https://doi.org/10.1016/j.rineng.2026.109755
Received 4 November 2025; Received in revised form 31 December 2025; Accepted 24 February 2026
Available online 24 February 2026

artifactual marginal bone loss, and the oral microflora differs markedly from humans. Moreover, although pigs and sheep provide ample bone volume, their narrow oral opening forces extra-oral surgical windows or osteotomies that bear no resemblance to clinical access, and the absence of a natural edentulous space prevents formation of a mucosal cuff or plaque milieu [6]. Rumination-driven acid–base shifts or spoon-shaped mandibles further risk cortical perforation and metabolic noise, rendering them poorly suited for soft-tissue-integration studies [7,8].

The rabbit model serves as a preferred preliminary platform for evaluating implant or grafting biomaterials before large-animal trials owing to the optimal anatomical proportionality, easy handling, rapid bone turnover, cost efficiency, and low ethical constraints [9,10]. As well-known extraoral implant sites, the rabbit tibia and femur offer a satisfactory bone volume for the standard-sized dental implant (Fig. 1A) [11–13]. However, distinct differences exist between intramembranous ossification (jawbone) and endochondral ossification (tibia and femur) in bone structure and remodeling dynamics, which result in unique biological responses and integration outcomes at the bone-implant interface [14]. In contrast, the intraoral implant model more closely mimics the integration dynamics of soft and hard tissues in clinical conditions [15]. A previous study notes that developing this model involves implant placement in the post–tooth-extraction socket, a procedure with several drawbacks including increased risks of tissue injury, extended modeling period for bone healing, and potential interference from occlusal forces during osseointegration (Fig. 1B) [16–19]. Edentulous diastema is an anatomical region between incisors and premolars in rabbits [20]. The bone volume of edentulous diastema in rabbit mandible is larger than maxilla, which also contains more trabecular bone, making it a promising site for implant placement [21]. Hence, we developed a intraoral transmucosal implant approach, positioning implants within the edentulous diastema of rabbits mandible [22,23].

Standardized animal models are critical to ensuring the validity and reproducibility of performance evaluation outcomes in preclinical studies of novel implant surface modifications and bone graft materials [18,24]. Despite anatomical and immunological disparities between animals and humans, ISO 10,993 regulations mandate rigorous in vivo testing of new dental implant materials to evaluate biocompatibility and functional efficacy before their clinical application in humans. Current research on rabbit intraoral implantation lacks standardized protocols for critical variables such as animal age, implant location, design, and surgical methodology [22,23,25]. This variability compromises the comparability and reproducibility of findings. Consequently, establishing a standardized intraoral implant model in the rabbit edentulous diastema—featuring anatomically precise positioning, consistent methodology, and high reproducibility—is essential to advance preclinical dental implant studies.

In this study, we standardized our previously established intraoral implant model by refining critical parameters: implant site selection, shape and size specifications, and surgical procedure. The standardized workflow circumvents tissue injury during tooth extraction, minimizes the modeling period and occlusal interference during osseointegration (Fig. 1C), and enables applicates in modeling the peri-implant mucositis and peri-implantitis. Beyond serving as an ideal platform for investigating the bone-implant interface and peri-implant infection, this model introduced a standardized, reproducible framework to assess novel dental implant coating modifications in preclinical functional analysis.

2. Material and methods

2.1. Workflow phase 1: pre-surgical planning & preparation

2.1.1. Ethical approval and animal standardization

All experimental protocols were approved by the Institutional Animal Care and Use Committee of Sun Yat-Sen University (No. SYSU-IACUC-2025–000,775) and conducted in compliance with ARRIVE guidelines. Thirty-seven male New Zealand White rabbits (2.0–2.5 kg) were sourced from a single licensed vendor (Guangdong Provincial Medical Experimental Animal Center) and housed under standard laboratory conditions with ad libitum access to food and water to minimize biological variability.

2.1.2. Anatomical standardization of the implant site

To define a reproducible implantation site, a detailed anatomical analysis of the mandibular edentulous diastema was first performed. Bilateral mandibles from euthanized rabbits ($n \geq 3$) were harvested, fixed in 4 % paraformaldehyde for 48 h, and scanned using high-resolution micro-CT (Skyscan 1276, Bruker; 15 μm isotropic voxel size, 70 kV, 114 μA). 3D reconstructions were analyzed to measure bucco-lingual bone width, mesio-distal length, and bone height within the diastema. This data was used to identify and standardize the optimal

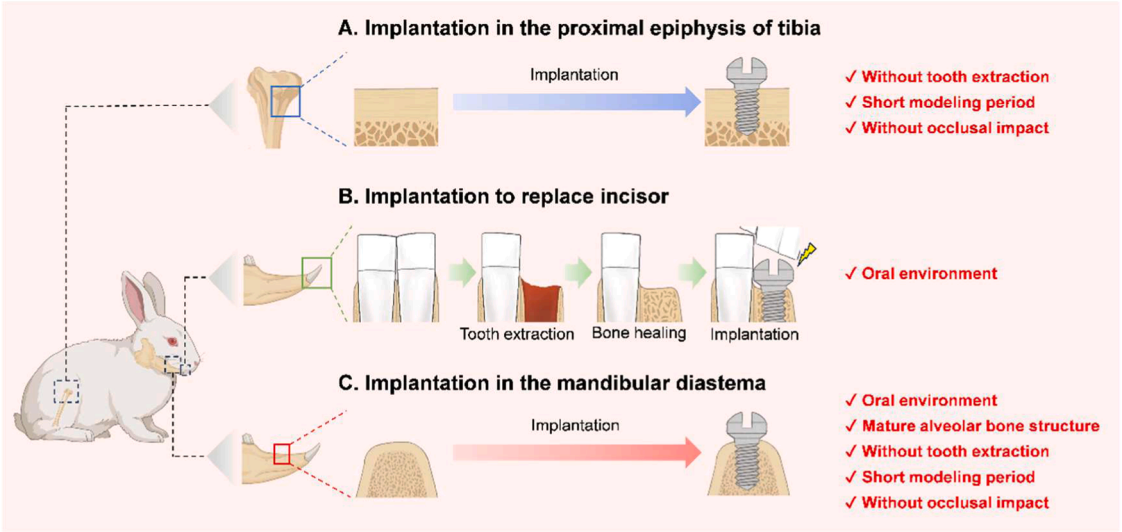

Fig. 1. Comparative schematic of extraoral vs. intraoral implant models in rabbits. (A) Tibial implant models circumvent the tooth extraction procedure offering a rapid modeling period and eliminating the risk of occlusal impact exposure, but it lacks oral environmental conditions. (B) Previous intraoral implant model offers an oral environment but demand tooth extraction and bone healing procedures before implantation. Additionally, the occlusal impact may risk model stability. (C) Intraoral implant model in edentulous diastema circumvents tooth extraction, bone healing procedure, and risk of occlusal impact exposure while offering oral environmental conditions, which is an optimal platform for implant biomaterial screening and osseointegration studies.

three-dimensional coordinates for implant placement, ensuring avoidance of critical anatomical structures.

2.1.3. Design and fabrication of customized implants

Titanium implants were custom-designed to match the anatomically defined bone volume. Each implant had a total length of 5.0 mm and a diameter of 1.6 mm, featuring a 2.0 mm smooth transmucosal collar and a 3.0 mm-long threaded endosseous portion with a 1.2 mm internal thread diameter. To standardize the osteogenic surface, all implants underwent uniform alkali-heat treatment: immersion in 5 M NaOH at 60 °C for 24 h, followed by gentle rinsing and heat treatment at 600 °C for 1 h to create a stable, micro-roughened bioactive titanium oxide layer.

2.2. Workflow phase 2: surgical implantation procedure

2.2.1. Anesthesia and aseptic preparation

Rabbits were anesthetized via intramuscular injection of a tiletamine-zolazepam (15 mg/kg) and xylazine (5 mg/kg) cocktail. Depth of anesthesia was confirmed by the loss of corneal and pedal reflexes. The animal was positioned supine, and the surgical field (perioral skin and oral cavity) was disinfected three times with povidone-iodine swabs followed by application of sterile drapes.

2.2.2. Standardized implant placement in the diastema

A longitudinal mucosal incision (~8–10 mm) was made along the crest of the edentulous diastema. Full-thickness mucoperiosteal flaps were reflected buccally and lingually to expose the bone. Using the predefined coordinates, the osteotomy was prepared sequentially under constant saline irrigation: a initial pilot drill was followed by drills with diameters of 1.0 mm, 1.2 mm, and 1.4 mm to a final depth of 3.0 mm. The custom implant was then manually inserted using a hand wrench until the implant shoulder was flush with the bone crest. Primary wound closure was achieved with interrupted 5–0 absorbable sutures.

2.3. Workflow phase 3: post-surgical model induction & maintenance

2.3.1. Standardized induction of peri-implant mucositis

Four weeks post-implantation, after soft tissue healing, localized inflammation was induced. The implant supra-structure was gently debrided with a sterile cotton tip. Using a micropipette, 5 μL of a standardized Staphylococcus aureus (ATCC 25,923) suspension (1 × 10^8 CFU/mL in PBS) was applied directly into the peri-implant sulcus. This procedure was repeated once weekly for 4 consecutive weeks. Oral hygiene measures were completely withdrawn for the duration of the induction period.

2.3.2. Standardized induction of peri-implantitis

Four weeks post-implantation, a ligature was placed to induce crestal bone loss. Under light sedation, a sterile #3–0 non-absorbable silk suture was carefully passed submarginally, wrapped twice around the implant neck, and secured with a surgical knot. Oral hygiene was discontinued. To accelerate and standardize bone loss, the ligature was replaced and apically displaced to the depth of the developing defect at 4 weeks post-ligation. The ligature remained in place until the study endpoint at 8 weeks post-initial ligation. In the peri-implantitis experiment, twelve rabbits were randomly assigned to sham or ligature groups ($n = 6$ per group). Within each group, three animals underwent micro-CT analysis and three underwent histological analysis.

2.3.3. Conventional incisor extraction model

Following the administration of tiletamine-zolazepam-xylazine for anesthesia, the rabbits were stabilized in a supine position. The oral cavity and perioral skin underwent routine disinfection with iodine swabs, followed by aseptic draping. The mandibular incisor was retracted with gauze to maximize exposure of the surgical site. The mucosa was incised at the distal axial angle of the mandibular incisor, and a mucosa separator was used to strip the labial and lingual mucosa from the bone surface. A small dental elevator was inserted into the mesial periodontal ligament region of the incisor and rotated clockwise to loosen the incisor. Dental forceps were then applied, and mesiodistal force was exerted to complete the extraction. The alveolar socket was scratched to remove residual tissue, and the alveolar bone was repositioned and compressed with aseptic cotton ball to stop bleeding.

2.4. Workflow phase 4: endpoint sampling & standardized analysis

2.4.1. Sample harvesting and preparation

At designated endpoints (osseointegration at 4/12 weeks, mucositis at 4 weeks, peri-implantitis at 8 weeks), animals were euthanized by anesthetic overdose. For Micro-CT & Histology: The mandibular segment containing the implant was dissected and fixed in 4 % paraformaldehyde for 48 h. For Molecular Analysis (RT-qPCR): Approximately 2 mm ring of peri-implant soft tissue was carefully excised, snap-frozen in liquid nitrogen, and stored at −80 °C.

2.4.2. Standardized analytical procedures

Micro-CT Analysis: Fixed specimens were scanned (Skyscan 1276; 90 kV, 200 μA). Two-dimensional images of the implants were obtained using Dataviewer software (v.1.5.6.2, Bruker) to measure the bone-to-implant contact (BIC) fraction at the implant threads. CTvox software (v.3.3.0, Bruker) was used for 3D reconstruction, and a 0.15-mm ring around the implant thread surface was defined as the region of interest to compare bone volume fraction (BV/TV), trabecular bone number (Tb. N), trabecular separation (Tb. Sp) and trabecular thickness (Tb. Th).

Histological analysis: Fixed samples were embedded in resin for non-decalcified sectioning or decalcified in 4 % EDTA for 12 weeks. Tissue resin blocks containing the implant and surrounding tissues were cut to a thickness of 300 μm using a diamond saw microtome (SP 1600, Leica) and then ground to a final thickness of 50 μm using a micro-grinding system (400 CS, EXAKT). The sections were stained with Van Gieson (G-clone) and Masson's trichrome (Solario) and observed under a stereomicroscope (MZ10F, Leica). Decalcified tissues were embedded in paraffin and cut into 4-μm sections for tartrate-resistant hydrochloric acid phosphatase (TRAP) staining (Servicebio). Peri-implant soft tissues were fixed in 4 % paraformaldehyde for 48 h and then embedded in paraffin. Sections were prepared and stained with Hematoxylin and eosin (H&E) staining solution (Biosharp). The images were captured using a slide scanner (Aperio AT2, Leica).

Reverse transcription quantitative polymerase chain reaction (RT-qPCR): After euthanizing the rabbits with peri-implantitis and peri-implant mucositis, 2-mm-wide peri-implant soft tissue were excised and stored in a −80 °C freezer for further experiments. Total RNA was extracted using RNAzol RT (Sigma-Aldrich). RNA concentration was measured using a Nanodrop spectrophotometer (Thermo Fisher). Complementary DNA (cDNA) was synthesized from 500 ng of total RNA using the PrimeScript RT Reagent Kit (Takara). Aliquots of the cDNA samples were loaded for RT-qPCR analysis in a 10 μL reaction using SYBR Green Premix (Takara) on a LightCycler 96 real-time PCR system (Roche). Expression levels of *IL6* and *CCL2* were detected. Gene expression was normalized to the reference gene glyceraldehyde 3-phosphate dehydrogenase (*GAPDH*) using the $2^{-\Delta\Delta Ct}$ method. Primer sequences were as follows: *GAPDH:* F–GTA TGA TTC CAC CCA CGG CA, R–CCA GCA TCA CCC CAC TTG AT; *Interleukin 6 (IL6):* F–GAC CAC GAT CCA CTT CA, R–AGG ATG GTG TGT TCT GAC CG; *Chemokine ligand 2 (CCL2):* F–GTC TCT GCA ACG CTT CTG TG, R–TTC TTT GGG ACA CTT GGT GCT.

2.5. Statistical analysis

All quantitative data are presented as mean ± standard deviation. Inter-group comparisons were performed using Student's *t*-test in GraphPad Prism 8.0.2. A p-value of < 0.05 was considered statistically

significant.

3. Results

3.1. Determination of the optimal implant site in rabbit edentulous diastema

To determine the optimal implantation site within the mandibular edentulous diastema of 3-month-old male New Zealand rabbits (2.0–2.5 kg), micro-CT imaging was employed to analyze the anatomical structure and available bone dimensions. The region of bone available for implant placement in the edentulous diastema is above the incisor roots. Notably, the mental nerve traverses this region and exits through the mental foramen, serving as a critical consideration factor during implant site selection and customized implant design (Fig. 2A). To pinpoint the optimal implant site, sagittal sections perpendicular to the edentulous diastema bone surface were analyzed (Fig. 2A1). The shortest distance (d) from these sections to the crown-root junction of the mandibular first premolar was determined. Within designated sagittal planes (Fig. 2A2-A5), the vertical bone height (h) was defined as the distance from the incisor root to the cortical surface, with coronal bone width designated as w1. Subsequent width measurements were recorded at depths of 1 mm (w2) and 2 mm (w3) apical to the coronal plane. Using these parameters, w and h were plotted against d (Fig. 2B). The vertical height (h) decreased initially, followed by a parabolic trend, correlating closely with the curvature of the incisor root. In most sections, w3 exceeded w1 and w2 due to the trapezoidal morphology of the bone above the incisors. However, w2 decreased within the d range of 2–5 mm due to the proximity of the mental foramen. Since the midline symphysis of the mandible is located anterior to the edentulous diastema, w1 increased sharply when d exceeded 16.5 mm, reflecting anatomical expansion at the mandibular junction.

Based on these findings, a micro-titanium implant with a 1.6 mm diameter, 3 mm threaded length, and 2 mm transmucosal height was designed (Fig. 2C, D). To ensure full osseous integration of the threaded structure, a minimum bone height (h) of 3 mm was required. Analysis identified $d = 7.50–10.50$ mm as the optimal range in which $h \geq 3$ mm (Fig. 2E). Thus, the edentulous region at 7.50–10.50 mm mesial to the

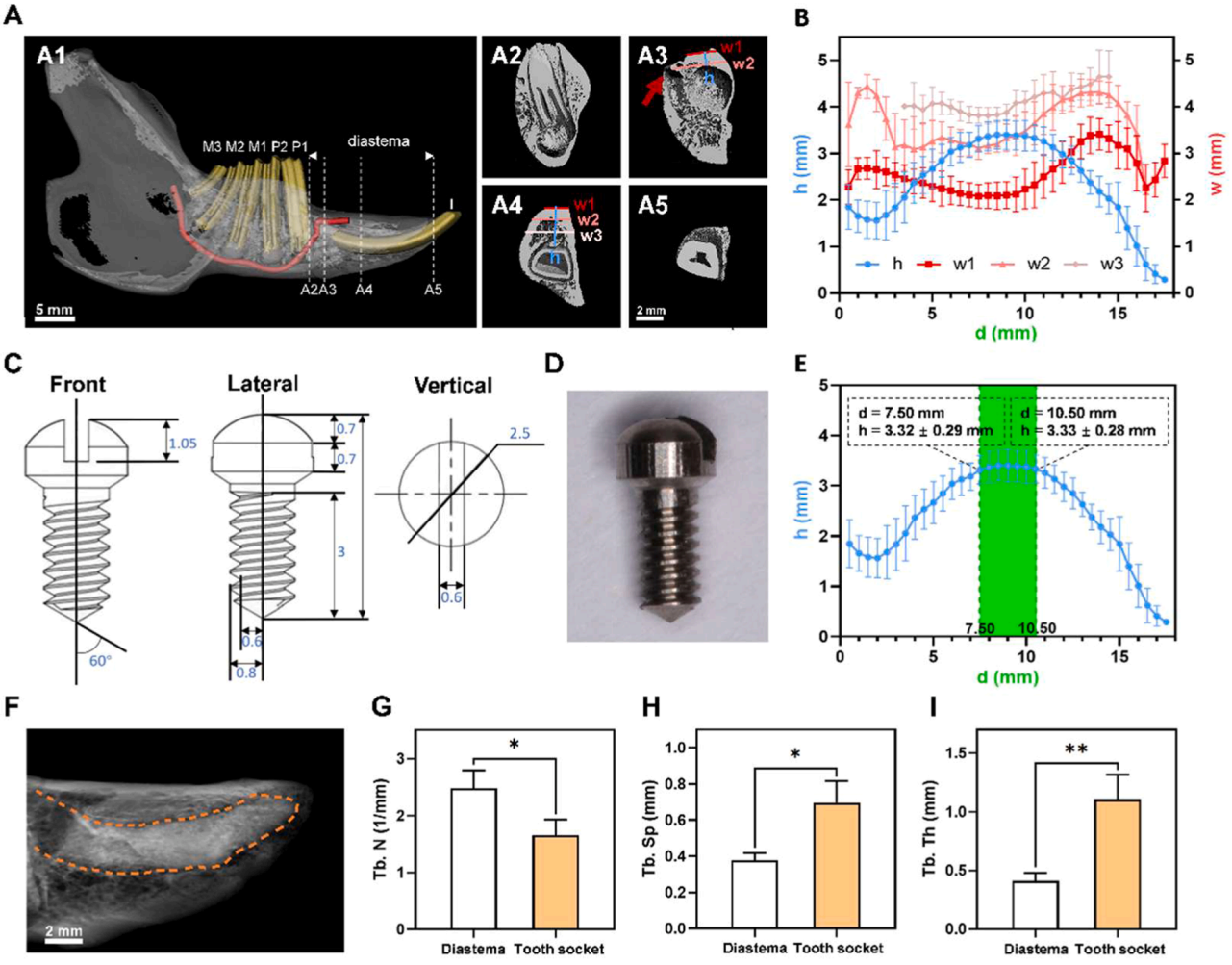

Fig. 2. Anatomical characterizations and bone analyses of the edentulous diastema in the mandible of New Zealand rabbit. (A) Three-dimensional reconstructed micro-CT images of the New Zealand rabbit mandible. Anatomical landmarks of mandibular teeth highlighted in yellow (P1: first premolar; P2: second premolar; M1: first molar; M2: second molar; M3: third molar; I: incisor) and the course of the inferior alveolar nerve indicated in red. White dashed-lines denote sagittal planes within the edentulous diastema (A1). Sagittal plane at the crown-root junction of the first premolar (A2). Sagittal plane at the mental foramen outlined by red arrow (A3). Sagittal plane through the mid-root of the incisor (A4). Sagittal plane at the midline symphysis (A5). (B) Trends in vertical bone height (h) and coronal/sub-coronal bone widths (w1, w2, w3) relative to the distance (d) from sagittal plane A2 ($n = 10$). (C) Schematic of the customized implant (1.6 mm diameter, 3 mm threaded length). (D) Macroscopic view of the implant. (E) Optimal implantation zone (7.50–10.50 mm from the crown-root junction of the mandibular first premolar) determined by $h \geq 3$ mm ($n = 10$). (F) Radiographic view of the incisor extraction socket (orange dashed-line) 4 weeks post-extraction. (G-I) Quantitative analysis of trabecular bone parameters including Tb. N, Tb. Sp, and Tb. Th in the diastema vs. extraction socket ($n = 3$; Student's t-test; * $P < 0.05$, ** $P < 0.01$). Error bar = standard deviation (SD); data are presented as mean values ± SD.

crown-root junction of the mandibular first premolar was selected for placement of the 3 mm threaded implant.

A comparative analysis of bone morphometric parameters was conducted between the previously described diastema (7.50–10.50 mm mesial to the mandibular first premolar) and the 4-week-healed extraction socket of incisors (Fig. 2F-I). Results demonstrated significantly higher Tb. N in the diastema implant site compared to the tooth socket, accompanied by reduced Tb. Sp and decreased Tb. Th (Fig. 2G-I). These findings suggest that the diastema exhibits a more mature trabecular architecture—characterized by denser, finer trabeculae with tighter spacing—compared to the healing tooth socket, rendering it biomechanically superior for dental implant placement.

3.2. Standardized workflow for rabbit intraoral implant model

A standardized surgical protocol was developed for implant placement within the rabbit mandibular edentulous diastema. The procedure involved sequential steps: (1) anatomical positioning, (2) mucosal incision, (3) pilot drilling for site localization, (4) osteotomy preparation, and (5) implant placement (Fig. 3A, B).

A male New Zealand rabbit was anesthetized by tiletamine-zolazepam-xylazine and positioned supine on modified cage-based operating platforms to optimize surgical access. The implant site positioning at the mandibular edentulous diastema—7.50–10.50 mm mesial to the crown-root junction of the first premolar—was performed using a periodontal probe, followed by local injection of adrenaline to reduce hemorrhage. Then 3.0 mm mesiodistal incision was made along the alveolar ridge, and full-thickness buccal/lingual flaps were reflected

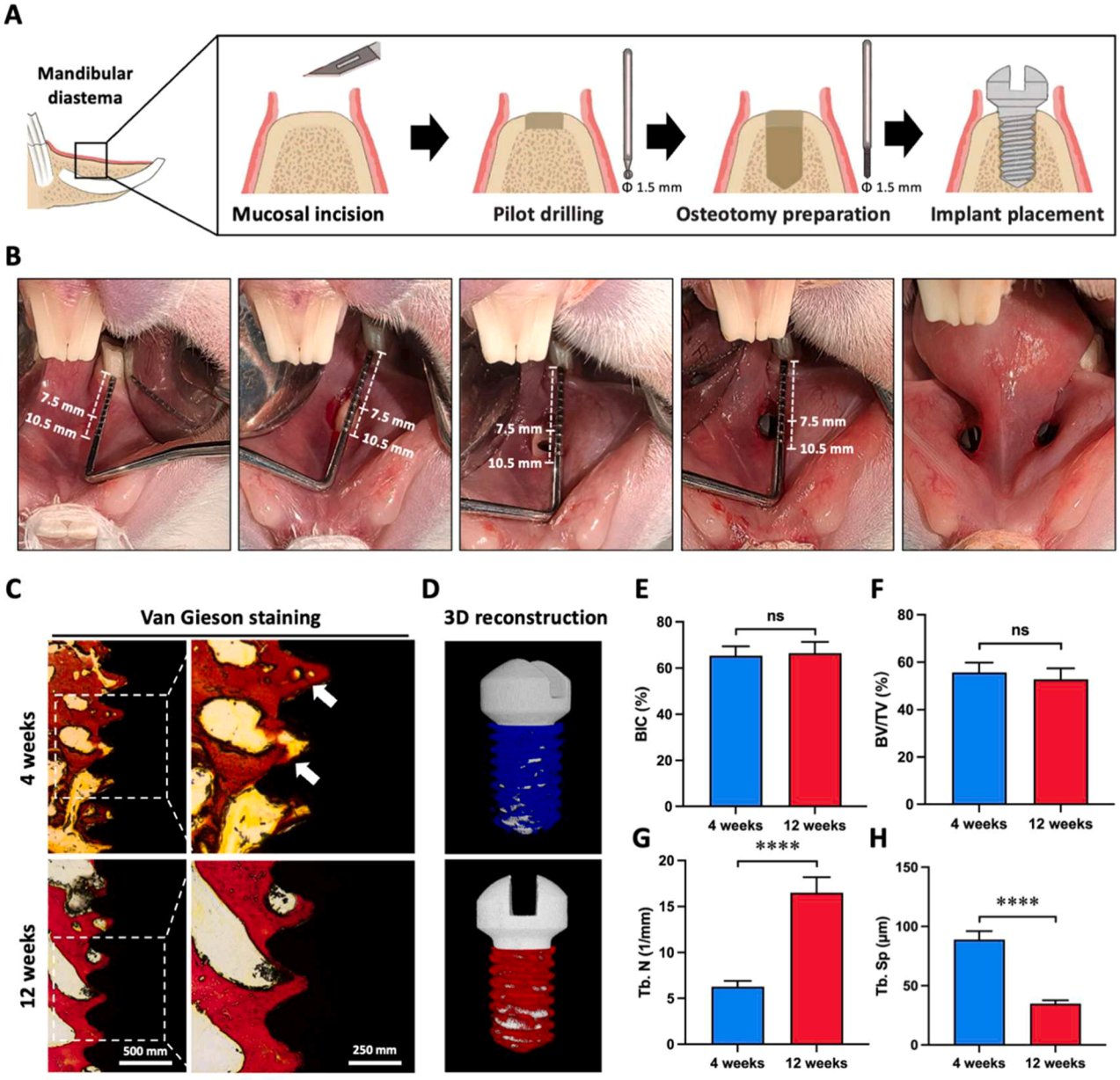

Fig. 3. Surgical workflow and osseointegration assessments. (A) Schematic of implant surgical workflow: site positioning, mucosal incision, pilot drilling, osteotomy preparation, and implant placement. (B) Photographic image of the standardized rabbit intraoral implant surgery (C) Van Gieson staining of 4- and 12-weeks after implantation, with white arrows indicating bone trabeculae within implant threads. (D) Micro-CT reconstruction of implants (white), peri-implant bone at 4 weeks (blue), and at 12 weeks (red). (E-H) Bone morphometry analysis including BIC, BV/TV, Tb. N, and Tb. Sp of peri-implant bone at 4 weeks and at 12 weeks ($n = 6$); Student's t-test; ** $P < 0.01$, *** $P < 0.001$; error bar = SD; data are presented as mean values ± SD.

with a gingival elevator to expose the cortical bone. With a micro-implant device, a 1.5 mm spherical drill was used to locate and create a pathway perpendicular to the bone surface, penetrating through the cortical bone, with saline cooling. A 1.5 mm tap drill was then inserted along the cortical pathway and manually tapped to the marked depth of 3 mm to prepare the implant site. The implant was first positioned with micro forceps. A screwdriver was then engaged with its coronal groove to manually advance the implant until all threads were fully seated within the bone. Finally, primary stability was verified using a calibrated torque wrench, achieving a consistent insertion torque of 15 Ncm for all implants. Postoperatively, penicillin (40,000 U/kg) was administered to prevent infection.

Utilizing meticulous positioning and stringent surgical protocols, mini-implants were successfully positioned 7.50–10.50 mm mesial to the first premolar in the mandibular edentulous diastema. The protocol ensured a clear surgical field with minimal tissue trauma, facilitating precise osseointegration and preserving adjacent anatomical structures.

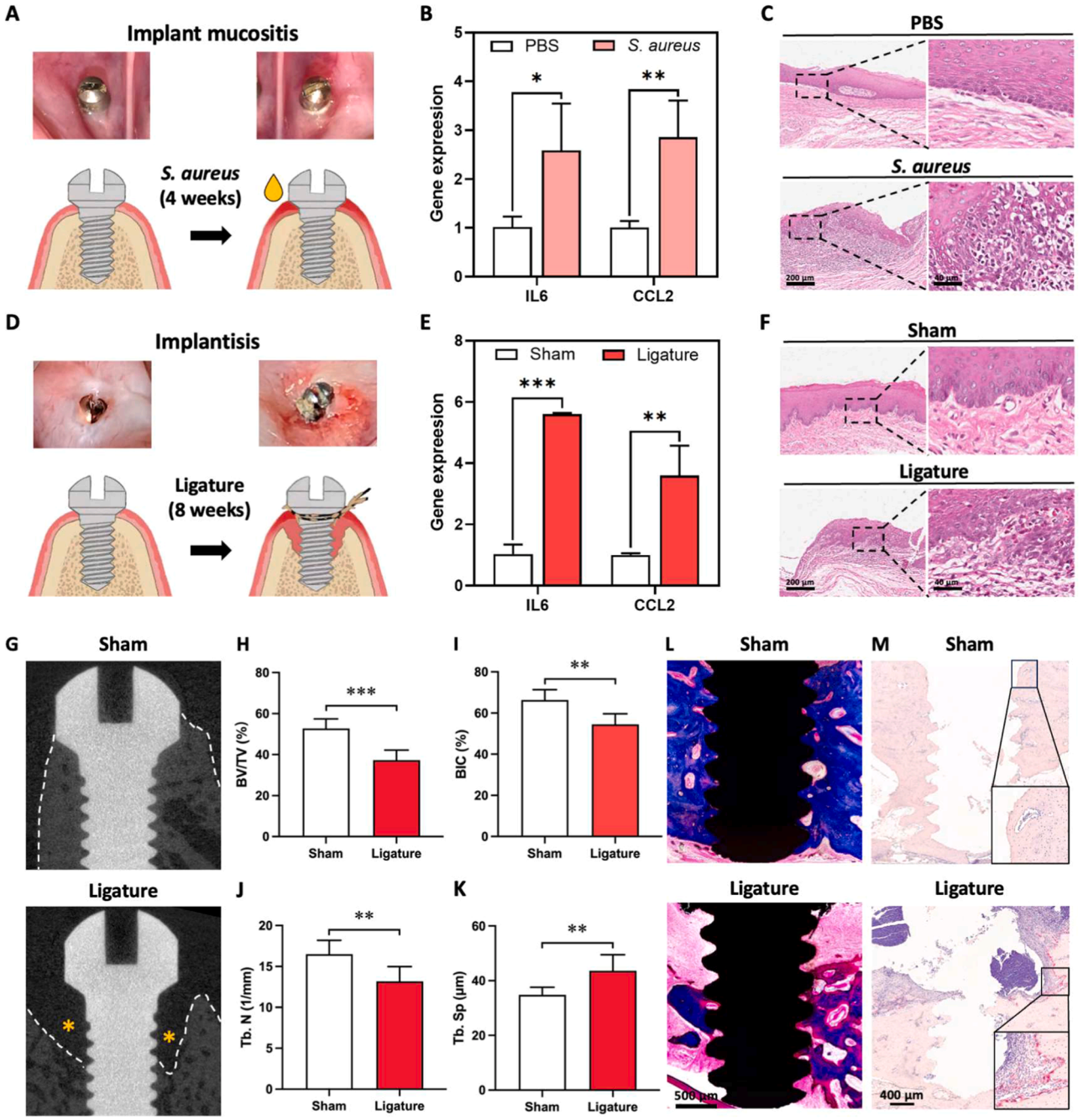

Fig. 4. Characterizations of peri-implant mucositis and peri-implantitis models. (A) Illustration for the establishment of *S. aureus*-induced peri-implant mucositis model. (B) RT-qPCR analysis demonstrating elevated mRNA levels of *IL6* and *CCL2* in the *S. aureus* group versus PBS group. (C) H&E staining of peri-implant soft tissues showing inflammatory infiltration in the *S. aureus* group. (D) Schematic of the ligature-induced peri-implantitis model. (E) Significant upregulation of *IL6* and *CCL2* mRNA in the ligature group compared to Sham group. (F) H&E staining of soft tissues: ligature group exhibited epithelial hyperplasia and inflammation, contrasting with control tissues. (G) Micro-CT 3D reconstructions of implants and peri-implant bone. (H-K) Quantitative analyses of bone parameters including BV/TV, BIC, Tb. N, and Tb. Sp. (L) Masson's trichrome staining revealing bone resorption in ligature group compared to Sham group. (M) TRAP staining showing osteoclast activity in two groups. $n = 6$; Student's *t*-test; * $P < 0.05$, ** $P < 0.01$, *** $P < 0.001$; error bar = SD; data are presented as mean values ± SD.

3.3. Evaluation of osseointegration in the standardized rabbit intraoral implant model

Osseointegration was evaluated at 4- and 12-weeks post-implantation using Van Gieson staining and micro-CT analysis (Fig. 3C—H). Van Gieson staining at 4 weeks and 12 weeks revealed that the cross-section of bone-implant contact (Fig. 3C). In the magnified view on the right side, white arrows indicate well-vascularized trabecular bone growing into the implant threads, confirming that osseointegration has already occurred one month after implant placement. This result highlights the advantage of the edentulous diastema of rabbits as dental implant model in shortening the implant osseointegration time. Micro-CT analysis at 12 weeks demonstrated comparable BIC and BV/TV to the 4-week timepoint. However, the Tb. N increased and Tb. Sp decreased significantly by 12 weeks, indicating enhanced trabecular maturation. These findings suggest that osseointegration is established within 4 weeks in the mandibular edentulous diastema, with continued trabecular refinement over time.

3.4. The standardized rabbit intraoral implant model for peri-implantitis modeling

We propose that this standardized rabbit intraoral implant model is a versatile tool for studying the pathogenesis of oral diseases, evaluating the biocompatibility of grafting materials, and accessing the performance of intraosseous implants. To exemplify the applicability, we utilized it for the peri-implant mucositis and peri-implantitis modeling.

Following a 4-week osseointegration period, two peri-implant infection models were developed on stable, integrated implants: *S. aureus*-induced mucositis model (Fig. 4A-C) and ligature-induced peri-implantitis model (Fig. 4D-L). We observed mucosal inflammation, gingival swelling, and plaque accumulation were observed in the peri- implant mucositis group (Fig. 4A). Molecularly, we confirmed elevated mRNA levels of inflammatory markers including *IL6* and *CCL2* in the peri- implant mucositis group (Fig. 4B). Accumulated inflammatory infiltrates were detected in gingival tissues of peri-implant mucositis group (Fig. 4C).

Furthermore, the mucosal erythema, swelling, and debris retention were detected in the 8-week ligated implants (Fig. 4D). The mRNA expression levels of *IL6* and *CCL2* were significantly upregulated (Fig. 4E). H&E staining showed hyperplastic epithelium and subepithelial inflammatory infiltration (Fig. 4F). Micro-CT revealed bone loss extending to the third thread of implant and trabecular degradation (Fig. 4G-K). Masson's trichrome staining confirmed that bone resorption occurred, with the original area being replaced by fibrous tissue (Fig. 4L). An evident infiltration of TRAP-positive osteoclasts was observed on the alveolar bone surface in the ligature group, indicating heightened bone resorptive activity. (Fig. 4M). Both models successfully mimicked clinical features of peri-implant diseases, indicating that the rabbit intraoral implant model can be applied to disease modeling via our standardized workflow, thereby providing a platform for studying infection mechanisms and testing therapeutic interventions.

We further evaluated implant retention in the peri-implantitis model (Table 1). Following a 4-week osseointegration period, all rabbits survived, with 22 of 24 implants remaining in place, yielding a retention rate of 92 %. Two implants were lost due to bone resorption: one rabbit's remaining implant underwent ligation, while the other served as an untreated control. In the remaining cohort, right-side implants were subjected to ligation, while left-side implants acted as controls. At the 4-week post-intervention assessment, three additional implants failed. One rabbit succumbed to anesthesia-related complications, resulting in the loss of two implants, and another implant in the ligation group was lost due to severe bone resorption. By the 8-week endpoint, all 10 surviving rabbits retained 18 implants, with no further losses. Excluding anesthesia-related attrition, the overall implant retention rate was 82 %.

4. Discussion

Current research priorities in implant dentistry emphasize surface modification strategies to optimize osseointegration and antimicrobial efficacy. Before translational application, novel implant or bone graft biomaterials must undergo rigorous preclinical validation in relevant animal models to assess biosafety, biocompatibility, antimicrobial efficacy, and osteogenic capacity. Hence, selecting an appropriate animal model requires a balanced consideration under the incorporation of research purpose, anatomical relevance, ethical compliance with animal welfare guidelines, and budgetary considerations [9,26]. Despite significant interspecies differences in skeletal anatomy, biomechanics, and metabolism, animal models remain critical for providing approximately mimicked human physiological and mechanical states in implant research, and each animal model has distinct advantages and limitations [26,27].

Large animal models (e.g., sheep, swine, non-human primates, and canines) are indispensable due to their clinical analogy to humans in key physiological, anatomical, and pathophysiological aspects [7,28,29]. For instance, the canine remains a gold-standard model in implant research due to their mandibular anatomy being congruence with humans, evidenced by comparable bone composition and density (canine: 1.2–1.5 g/cm^3 vs. human: 1.1–1.3 g/cm^3) and bone remodeling dynamics, with annual turnover rates of 5.2 $\pm$ 0.8 % in canines and 3.7 $\pm$ 0.6 % in humans [30,31]. In addition to anatomical similarities, these large experimental animals also have the advantage of sufficient bone volume and the ability to simulate functional occlusal loads (200–300 N), making them ideal animal models for evaluating the loading of standard-sized dental implants used in clinical practice [32,33]. However, high breeding costs, limited availability of related biological reagents, and low social acceptance of large animal model experiments restrict their use in exploring of molecular mechanisms [34].

Small animal models (e.g., mouse and rat) provide invaluable insights into human genetic disorders and fundamental physiological mechanisms. However, translational research outcomes from these systems may not always translate directly to clinical settings. While cost-effective rodent models like mice circumvent ethical concerns associated with large animals, their severely restricted mandibular bone volume

Table 1
Implant retention rate at different time point.

Time (week)	Event	Survival	Death	Remaining implants (stable: mobile)	Loss of implants
0	Implantation	12	0	24:0 (Sham: 12; Ligature:12)	/
4	Ligature	12	0	24:0 (Sham: 10; Ligature:11; Excluded 1)	2(2: insufficient primary stability)
8	Ligature replacement	11	1 (ancsthcisa-related mortailty)	18:0 (Sham:9; Ligature:9)	3(2: ansthcsia-related moratality; 1:bone resoption)
12	Sacifice	11	0	18:0 (Sham:9; Ligature:9)	/
				4th week (osseointegration)	12th week (endponit of ligature)
Implant retention rate				92 %	75 %
Implant retention rate (exclude anesthesia-related loss)				92 %	82 %

presents critical limitations: (1) Maximum implant diameter thresholds (≤1.5 mm) constrain device design [35,36]; (2) Elevated intraoperative fracture risks frequently cause cortical perforations, damaging adjacent anatomical landmarks [24]; (3) Biomechanical instability under functional loading [18]. Furthermore, accelerated bone turnover rates and hyperactive osteoclastogenesis fundamentally alter remodeling patterns. Consequently, mouse and rat models are more suitable for assessing the toxicity and biocompatibility of various implant materials [26].

Rabbits are commonly used to test dental implants and the biological and biomechanical aspects of osseointegration. The macrostructure of rabbit bone differs from that of humans, featuring primary vascular osteons aligned parallel to the bone axis, surrounding the medullary canal and periosteum, with dense Haversian bone in between [10]. Compared to primates and some large animals, rabbits exhibit faster skeletal adaptation and bone turnover, driven by active intracortical Haversian remodeling [37,38]. Nevertheless, there are some similarities in bone composition and density between rabbits and humans [10]. The edentulous diastema, a relatively long toothless region between the incisor and the premolar in rabbits, is considered a promising site for implant fixation [25].

This study assessed the anatomical and biological viability of the edentulous diastema in New Zealand white rabbits as an intraoral implant site. The optimal implantation site was identified as 7.50–10.50 mm mesial to the crown-root junction of the mandibular first premolar, characterized by elevated trabecular bone density and sufficient bone volume. Experimental implants (1.6 mm diameter, 3 mm threaded length, 2 mm transmucosal height) were designed based on morphometric analysis, following a standardized surgical protocol. The implants' threaded structure and alkali-heat-treated rough surface enhanced initial stability [39], achieving a 90 % retention rate and > 60 % BIC at 4 weeks post-implantation, compliant with ISO 10,993–6: 2021 biocompatibility standards. Following ligature-induced peri-implantitis, 80 % implant retention was maintained at 8 weeks, demonstrating that 3 mm of osseointegration resists infection-driven bone resorption. Notably, no mandibular fractures occurred, underscoring procedural safety. Although standard-sized clinical implants cannot be accommodated in rabbits, this model achieved robust osseointegration and is suitable for preclinical evaluation of surface-modified implants, bridging translational gaps in dental biomaterial research.

Standardizing this model is critical for improving interstudy comparability and ensuring experimental precision. To achieve this, rigorous inclusion criteria were applied during the selection of New Zealand white rabbits, minimizing variability in mandibular bone volume caused by age, sex, and weight. Given estrogen's central role in regulating bone remodeling (balancing osteogenesis and osteolysis), male rabbits were selected to eliminate sex-related hormonal influences [40]. Additionally, to account for age- and weight-dependent increases in bone volume, animals were restricted to 3 months of age and 2.0–2.5 kg body weight, ensuring consistent anatomical reference points and reproducibility [41]. Further standardization was achieved through implant design and surgical protocols. Customized implants were tailored to the bone volume of the target site, with dimensions optimized to minimize tissue trauma while enhancing procedural uniformity. Detailed surgical guidelines were established, including the use of periodontal probes and precision drills to mark implant sites, thereby reducing operator-dependent variability. These measures collectively improved surgical consistency, reduced heterogeneity, and strengthened the model's utility for cross-study validation. Future research should include a direct comparison between the tooth-extraction socket implantation model and the diastema implantation model. The present study is methodological in nature, with its advantage lying in the establishment of an anatomically standardized, extraction-free intraoral experimental site protocol. This protocol features a shorter experimental duration than the extraction-based model, because diastema implantation allows for direct implant placement without the need to wait for the healing of the extraction socket.

5. Conclusions

To sum up, through detailed anatomical analysis of the edentulous diastema of the New Zealand white rabbit, we identified optimal implant sites, designed customized implants, and standardized the operative workflow. This standardized model offers several advantages: it mimics the oral environment, circumvents the requirement of tooth extraction, minimizes tissue injury, and simplifies procedural steps. Leveraging this model, we successfully developed two preclinical infection models: an *S. aureus*-induced peri-implant mucositis model and a ligature-induced peri-implantitis model. The standardized intraoral implant model in rabbit edentulous diastema facilitates mechanistic investigations into osseointegration and peri-implant infectious processes while enabling preliminary assessments of material functionality and safety-critical steps that can accelerate translational advancements in implant research.

Two key limitations are noted: the small sample size inherent to a standardized animal model that could influence statistical robustness, and the anatomical necessity for mini-implants, thereby constraining direct biomechanical extrapolation to human-scale devices. Nevertheless, this approach provides a highly reproducible, economical, and effective platform for fundamental inquiries into osseointegration, the evaluation of novel implant surface coatings, and the initial screening of biomaterials, even if it is not suitable for modeling the functional loading.

CRediT authorship contribution statement

Xinning Dai: Writing – original draft, Visualization, Validation, Methodology, Investigation, Formal analysis, Data curation, Conceptualization. **Xiaoqiong Huang:** Writing – original draft, Visualization, Validation, Methodology, Investigation, Formal analysis, Data curation, Conceptualization. **Xinwen Deng:** Writing – review & editing, Visualization, Validation, Methodology, Investigation, Formal analysis, Data curation. **Zhiqian Ye:** Writing – review & editing, Visualization, Validation, Methodology, Investigation, Formal analysis, Data curation. **Zixiang Liu:** Writing – review & editing, Visualization, Validation, Methodology, Investigation, Formal analysis, Data curation. **Weiran Li:** Writing – review & editing, Validation, Methodology, Investigation, Formal analysis, Data curation. **Yan Li:** Writing – review & editing, Supervision, Project administration, Funding acquisition, Conceptualization. **Shuyi Wu:** Writing – review & editing, Supervision, Project administration, Funding acquisition, Conceptualization. **Shujin Li:** Writing – review & editing, Supervision, Project administration, Funding acquisition, Conceptualization.

Declaration of competing interest

The authors declare that they have no known competing financial interests or personal relationships that could have appeared to influence the work reported in this paper.

Acknowledgements

This work was supported by the National Natural Science Foundation of China (82271031 and 82571158), the National Outstanding Young Physician Program, the Guangdong Basic and Applied Basic Research Foundation (2024A1515010833 and 2026A1515012845), the Science and Technology Program of Guangzhou, China (SL2024A04J01058), and the Postdoctoral Fellowship Program of China Postdoctoral Science Foundation (GZC20251214).

Data availability

No data was used for the research described in the article.

References

[1] E. Marin, F. Boschetto, G. Pezzotti, Biomaterials and biocompatibility: an historical overview, J. Biomed. Mater. Res. A 108 (2020) 1617–1633.
[2] S. Stubinger, M. Dard, The rabbit as experimental model for research in implant dentistry and related tissue regeneration, J. Invest. Surg. 26 (2013) 266–282.
[3] J. Wu, J. Deng, G. Theocharidis, T.L. Sarrafian, L.G. Griffiths, R.T. Bronson, A. Veves, J. Chen, H. Yuk, X. Zhao, Adhesive anti-fibrotic interfaces on diverse organs, Nature 630 (2024) 360–367.
[4] H.C. Lim, K.S. Lee, S.Y. Shin, R.E. Jung, U.W. Jung, D.S. Thoma, Effects of implant placement timing and type of soft-tissue grafting on histological and histomorphometric outcomes in a preclinical canine model, J. Clin. Periodontol. 51 (2024) 840–851.
[5] S. Battula, J.W. Lee, H.B. Wen, S. Papanicolaou, M. Collins, G.E. Romanos, Evaluation of different implant designs in a ligature-induced peri-implantitis model: a canine study, Int. J. Oral Maxillofac. Implants 30 (2015) 534–545.
[6] N. Areid, J. Willberg, I. Kangasniemi, T.O. Narhi, Organotypic in vitro block culture model to investigate tissue-implant interface. An experimental study on pig mandible, J. Mater. Sci. Mater. Med. 32 (2021) 136.
[7] S. Shanbhag, J. Sanz-Esporrin, C. Kampleitner, S.A. Lie, R. Gruber, K. Mustafa, M. Sanz, Peri-implant bone regeneration in pigs, Int. J. ImPlant Dent. 10 (2024) 55.
[8] S. Ernst, S. Stubinger, P. Schupbach, M. Sidler, K. Klein, S.J. Ferguson, B. von Rechenberg, Comparison of two dental implant surface modifications on implants with same macrodesign: an experimental study in the pelvic sheep model, Clin. Oral Implants Res. 26 (2015) 898–908.
[9] A.I. Pearce, R.G. Richards, S. Milz, E. Schneider, S.G. Pearce, Animal models for implant biomaterial research in bone: a review, Eur. Cell Mater. 13 (2007) 1–10.
[10] M. Mapara, B.S. Thomas, K.M. Bhat, Rabbit as an animal model for experimental research, Dent. Res. J. (Isfahan) 9 (2012) 111–118.
[11] C.L. Hatley, S.M. Cameron, M.F. Cuenin, M.H. Parker, S.H. Thompson, S.B. Harvey, The effect of dental implant spacing on peri-implant bone using the rabbit (Oryctolagus cuniculus) tibia model, J. Prosthodont. 10 (2001) 154–159.
[12] X. Zhou, J. Jiang, J. Dang, Y. Wang, R. Hu, C. Shen, T. Zhao, D. Sun, G. Wang, M. Zhang, Intelligent supramolecular modification for implants: endogenous regulation of bone defect repair in osteoporosis, Adv. Mater. 36 (2024) e2406227.
[13] D. Reinedahl, S. Galli, T. Albrektsson, P. Tengvall, A. Wennerberg, Aseptic silk ligatures induce bone resorption around titanium implants: a 12-week pilot study in rabbits, Int. J. Oral Maxillofac. Implants 39 (2024) 755–764.
[14] A.D. Berendsen, B.R. Olsen, Bone development, Bone 80 (2015) 14–18.
[15] N. Blanc-Sylvestre, P. Bouchard, C. Chaussain, C. Bardet, Pre-clinical models in implant dentistry: past, present, future, biomedicines, 9 (2021).
[16] M.B. Guglielmotti, D.G. Olmedo, R.L. Cabrini, Research on implants and osseointegration, Periodontol 2000 (79) (2019) 178–189.
[17] I.N. Safi, B.M.A. Hussein, A.M. Al-Shammari, Bio-hybrid dental implants prepared using stem cells with beta-TCP-coated titanium and zirconia, J. Periodontal. ImPlant Sci. 52 (2022) 242–257.
[18] N.M. AlOtaibi, M. Dunne, A.F. Ayoub, K.B. Naudi, A novel surgical model for the preclinical assessment of the osseointegration of dental implants: a surgical protocol and pilot study results, J. Transl. Med. 19 (2021) 276.
[19] Z. Shen, Y. Xu, X.N. Qian, Y.H. Zhou, Y. Zhou, J.Y. Zhou, Y. Liu, S.M. Zhang, J. Qiu, Enhanced osteogenic and antibacterial properties of titanium implant surface modified with Zn-incorporated nanowires: preclinical in vitro and in vivo investigations, Clin. Oral Implants Res. 35 (2024) 427–442.
[20] T.M. Donnelly, D. Vella, Anatomy, physiology and non-dental disorders of the mouth of pet rabbits, Vet. Clin. North Am. Exot. Anim. Pract. 19 (2016) 737–756.
[21] V.E. Campillo, S. Langonnet, A. Pierrefeu, A.G. Chaux-Bodard, Anatomic and histological study of the rabbit mandible as an experimental model for wound healing and surgical therapies, Lab. Anim. 48 (2014) 273–277.
[22] W. Li, Z. Huang, X. Li, M. Zhang, Q. Li, S. Luo, Y. Li, D. Wu, S. Wu, Coral-inspired anti-biofilm therapeutic abutments as a new paradigm for prevention and treatment of peri-implant infection, SmartMat 5 (2024) e1284.
[23] S. Wu, J. Xu, L. Zou, S. Luo, R. Yao, B. Zheng, G. Liang, D. Wu, Y. Li, Long-lasting renewable antibacterial porous polymeric coatings enable titanium biomaterials to prevent and treat peri-implant infection, Nat. Commun. 12 (2021) 3303.
[24] X. Liu, S. Deng, X. Li, H. Liu, Z. Li, Y. Wu, P. Luo, X. Zhong, R. Huang, R. Liu, X. Wu, B. Huang, Z. Chen, Z. Chen, S. Chen, A standardized rat model to study peri-implantitis of transmucosal osseointegrated implants, Biomater. Res. 28 (2024) 0021.
[25] M.A. Alkhodary, Effect of controlled surface roughness and biomimetic coating on titanium implants adhesion to the bone: an experiment animal study, Saudi. Dent. J. 35 (2023) 819–826.
[26] A. Scarano, A.G.A. Khater, S.A. Gehrke, F. Inchingolo, S.R. Tari, Animal models for investigating osseointegration: an overview of implant research over the last three decades, J. Funct. Biomater. (2024) 15.
[27] D. Yin, S. Zhan, Y. Liu, L. Yan, B. Shi, X. Wang, S. Zhang, Experimental models for peri-implant diseases: a narrative review, Clin. Oral Investig. 28 (2024) 378.
[28] J. Lindhe, T. Berglundh, I. Ericsson, B. Liljenberg, C. Marinello, Experimental breakdown of peri-implant and periodontal tissues. A study in the beagle dog, Clin. Oral Implants Res. 3 (1992) 9–16.
[29] F. Schwarz, A. Sculean, S.P. Engebretson, J. Becker, M. Sager, Animal models for peri-implant mucositis and peri-implantitis, Periodontol 2000 (68) (2015) 168–181.
[30] E.G. Vajda, M. Kneissel, B. Muggenburg, S.C. Miller, Increased intracortical bone remodeling during lactation in beagle dogs, Biol. Reprod. 61 (1999) 1439–1444.
[31] F. Vignoletti, I. Abrahamsson, Quality of reporting of experimental research in implant dentistry. Critical aspects in design, outcome assessment and model validation, J. Clin. Periodontol. 39 (Suppl 12) (2012) 6–27.
[32] A. Kozlovsky, H. Tal, B.Z. Laufer, R. Leshem, M.D. Rohrer, M. Weinreb, Z. Artzi, Impact of implant overloading on the peri-implant bone in inflamed and non-inflamed peri-implant mucosa, Clin. Oral Implants Res. 18 (2007) 601–610.
[33] J.L. Calvo-Guirado, A. Aguilar-Salvatierra, G. Gomez-Moreno, J. Guardia, R. A. Delgado-Ruiz, J.E. Mate-Sanchez de Val, Histological, radiological and histomorphometric evaluation of immediate vs. non-immediate loading of a zirconia implant with surface treatment in a dog model, Clin. Oral Implants Res. 25 (2014) 826–830.
[34] A. Kantarci, H. Hasturk, T.E. Van Dyke, Animal models for periodontal regeneration and peri-implant responses, Periodontol. 2000 68 (2015) 66–82.
[35] T. Koutouzis, C. Eastman, S. Chukkapalli, H. Larjava, L. Kesavalu, A novel rat model of polymicrobial peri-implantitis: a preliminary study, J. Periodontol. 88 (2017) e32–e41.
[36] S. Deng, Y. Hu, J. Zhou, Y. Wang, Y. Wang, S. Li, G. Huang, C. Peng, A. Hu, Q. Yu, X. Han, TLR4 mediates alveolar bone resorption in experimental peri-implantitis through regulation of CD45(+) cell infiltration, RANKL/OPG ratio, and inflammatory cytokine production, J. Periodontol. 91 (2020) 671–682.
[37] T. Taguchi, M.J. Lopez, An overview of de novo bone generation in animal models, J. Orthop. Res. 39 (2021) 7–21.
[38] S. Castaneda, R. Largo, E. Calvo, F. Rodriguez-Salvanes, M.E. Marcos, M. Diaz-Curiel, G. Herrero-Beaumont, Bone mineral measurements of subchondral and trabecular bone in healthy and osteoporotic rabbits, Skeletal. Radiol. 35 (2006) 34–41.
[39] D.D. Bosshardt, V. Chappuis, D. Buser, Osseointegration of titanium, titanium alloy and zirconia dental implants: current knowledge and open questions, Periodontol. 2000 73 (2017) 22–40.
[40] M. Almeida, M.R. Laurent, V. Dubois, F. Claessens, C.A. O'Brien, R. Bouillon, D. Vanderschueren, S.C. Manolagas, Estrogens and androgens in skeletal physiology and pathophysiology, Physiol. Rev. 97 (2017) 135–187.
[41] M. Kanekawa, N. Shimizu, Age-related changes on bone regeneration in midpalatal suture during maxillary expansion in the rat, Am. J. Orthod. Dentofacial Orthop. 114 (1998) 646–653.